Chemistry–A European Journal
Research Article
doi.org/10.1002/chem.202104260
Chemistry Europe
European Chemical Societies Publishing
www.chemeurj.org

Sigma/pi Bonding Preferences of Solvated Alkali-Metal Cations to Ditopic Arylmethyl Anions

Annabel Rae,[a] Keelan M. Byrne,[b] Scott A. Brown,[a] Alan R. Kennedy,[a] Tobias Krämer,*[b, c] Robert E. Mulvey,[a] and Stuart D. Robertson*[a]

Abstract: Arylmethyl anions allow alkali-metals to bind in a σ-fashion to the lateral carbanionic centre or a π-fashion to the aryl ring or in between these extremities, with the trend towards π bonding increasing on descending group 1. Here we review known alkali metal structures of diphenylmethane, fluorene, 2-benzylpyridine and 4-benzylpyridine. Next, we synthesise Li, Na, K monomers of these diarylmethyls using polydentate donors PMDETA or Me_6TREN to remove competing oligomerizing interactions, studying the effect that two aromatic rings has on negative charge (de)localisation via NMR, X-ray crystallographic and DFT studies. Diphenylmethyl and fluorenyl anions maintain C(H)–M interactions regardless of alkali-metal, although the adjacent arene carbons engage in interactions with larger alkali-metals. Introducing a nitrogen atom into the ring (at the 2- or 4-position) encourages relocalisation of negative charge away from the deprotonated carbon and onto nitrogen. Phenyl(2-pyridyl)methyl moves from an enamide formation at one extremity (lithium) to an aza-allyl formation at the other extremity (potassium), while *C*- or *N*-coordination modes become energetically viable for Na and K phenyl(4-pyridyl)methyl complexes.

Introduction

Organoalkali-metal chemistry has historically been dominated by the lightest member of the group, lithium,[1] in part on account of the typically increased solubility of organolithium reagents in non-polar organic solvents with respect to their heavier counterparts.[2] Furthermore, as strong nucleophiles, bases, or ligand transfer agents, organolithium reagents have provided synthetic chemists with sufficient reactivity to warrant them being the first port of call for many organic transformations. However, heavier alkali-metal chemistry (particularly sodium and potassium) is currently undergoing a resurgence[3] for sustainability reasons on account of their higher earth abundance.[4] This is driven in part by the increased demand for lithium as the market for rechargeable batteries is rapidly expanding,[5] with governments across the globe setting increasingly aggressive targets for the widespread replacement of combustion engine powered vehicles with electric vehicles.[6]

One feature of these heavier alkali-metals which provides an important distinction from lithium is the much greater steric accessibility to coordinate to the π(pi)-systems of aromatic rings. While this π-philicity of the heavier alkali-metals has long been recognised it is now in sharper focus due to the role of such metal-π aromatic interactions for the stabilisation of highly reactive low-valent main group species[7] or products of small molecule activation.[8] We have had a long-standing interest in the structural study of alkali-metal complexes with organic anions which present an opportunity to engage in σ or π (or both) interactions with the metal (Figure 1).[9] Our approach is to target (highly sensitive) monomers where possible as this strips out any secondary interactions which facilitate oligomerization and thus removes any aggregation effects which are present. While our previous structural studies have assessed benzyl (**1**) 2-picolyl (**2**) and 4-picolyl (**3**) anions, here we extend this research to those which contain greater aromatic substitution [that is to replace one hydrogen atom of CH_2 arms with a Ph ring, specifically in diphenylmethyl [Ph_2CH^-, **4**], fluorenyl [$(C_6H_4)_2CH^-$, **5**], phenyl(2-pyridyl)methyl [$(Ph)(2\text{-}C_5H_4N)CH^-$, **6**] and phenyl(4-pyridyl)methyl [$(Ph)(4\text{-}C_5H_4N)CH^-$, **7**] to gain an understanding of the effect that an additional aromatic group has on the bonding and overall charge delocalization within such complexes (see Figure 2 for structures of protonated substrates).

Putting into context the new complexes and their crystal structures reported here, we commence by briefly summarizing the previously known crystallographically characterised alkali-metal complexes of these ligands **4**–**7**.

[a] *A. Rae, S. A. Brown, Dr. A. R. Kennedy, Prof. R. E. Mulvey, Dr. S. D. Robertson*
WestCHEM, Department of Pure and Applied Chemistry
University of Strathclyde
295 Cathedral Street, Glasgow, G1 1XL (UK)
E-mail: stuart.d.robertson@strath.ac.uk

[b] *K. M. Byrne, Dr. T. Krämer*
Department of Chemistry
Maynooth University
W23 F2H6 Maynooth, Co Kildare (Ireland)
E-mail: tobias.kraemer@mu.ie

[c] *Dr. T. Krämer*
Hamilton Institute
Maynooth University
W23 A3HY Maynooth, Co Kildare (Ireland)

Supporting information for this article is available on the WWW under https://doi.org/10.1002/chem.202104260

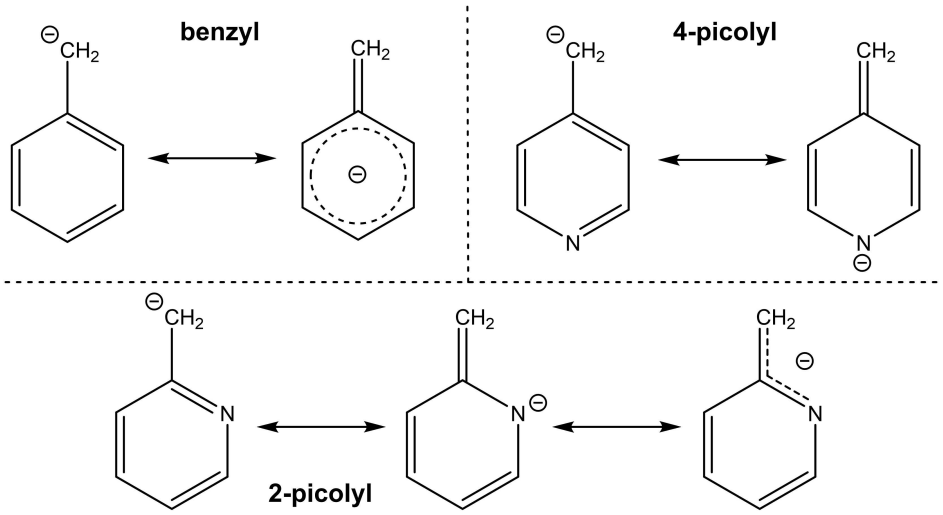

Figure 1. Potential resonance forms available to benzyl (**1**, top left), 2-picolyl (**2**, bottom) and 4-picolyl (**3**, top right) anions.

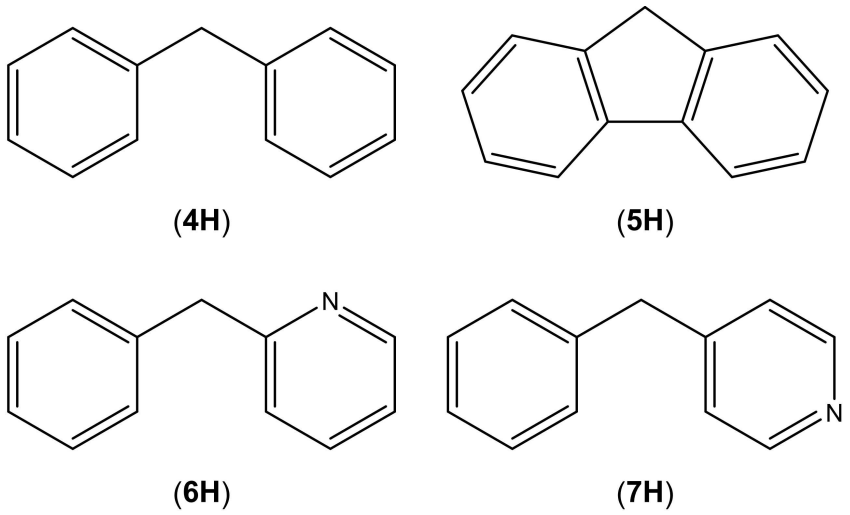

Figure 2. Parent precursors of the anions studied in this work; diphenylmethane (**4H**); fluorene (**5H**); 2-benzylpyridine (**6H**) and 4-benzylpyridine (**7H**).

The structural chemistry of these four ligands is dominated by diphenylmethyl and fluorenyl complexes (see Table 1 for a complete list of crystallographically characterized alkali-metal complexes of these four ligands). Both anions are comfortable adopting solvent-separated ion pairs (SSIP) in the presence of Lewis donors such as crown-ethers, cryptands or diglyme (DG) which are adept at sequestering alkali-metal counteranions.[10] This demonstrates the ease with which these two anions can delocalize negative charge away from the formally deprotonated α-carbon atom. This is expected especially for the fluorenyl anion since it contains an aromatic cyclopentadienyl (Cp) core with two further fused aromatic rings which can help dissipate the negative charge further. Rather than use the inner five-membered ring, an outer ring can be used exclusively to bind to large, soft potassium when surrounded by 18-crown-6, which leaves a vacant site at the apex of potassium in monomeric **5K·18-c-6**.[10b] The other Lewis donors THF, dimethoxyethane or pyridine can then occupy this vacant site, bridging between two of these 18-crown-6 solvated fluorenylpotassium units to give dinuclear complexes.[10b,11]

Unsolvated complexes are rare, with only fluorenyllithium[12] and fluorenylsodium[13] reported. The former dimerizes (**[5Li]$_2$**), again using the outer aromatic rings to bind to the metal in a η^6 fashion, with the two ligands lying in an antiparallel manner with respect to each other to create a double sandwich for their metal guests (Figure 3). The larger ionic radius of sodium allows it to bridge three fluorenyl anions, resulting in a polymer **[5Na]**$_\infty$ perhaps better described as **[Na$_2$(5$_3$Na)]**$_\infty$ on account of the two distinct Na environments; the unique Na is surrounded by three η^1 (C_α) coordinated fluorenyl anions in a propeller-like fashion with a short Na–C bond length of 2.483(3) Å, with the remaining two 'naked' Na cations weakly coordinating three C_6 rings (Figure 3).

Table 1. Summary of crystallographically characterized alkali-metal complexes of ligands **4**–**7**.

Ligand	M	Donor	Aggregation	Metal C.N. (donor)	M-L coord	Formula	Ref
Ph_2CH (**4**)	Li	12-crown-4	SSIP	8	–	**$[Li{\cdot}(12\text{-}c\text{-}4)_2]^+[4]^-$**	10a
	Na	TMEDA	Tetramer	2 (M1) 2 (M2)	$\eta^1(C_\alpha)$, $\eta^1(C_\alpha)$ $\eta^1(C_\alpha)$, η^2 (Ph)	**$[4Na{\cdot}TMEDA]_4$**	18
		PMDETA	Monomer	3	η^5 (C_o-C_i-C_α-$C_{i'}$-$C_{o'}$)	**4Na·PMDETA**	18
	K	THF	Polymer	1	$\eta^1(C_\alpha)$, $\eta^1(C_\alpha)$, η^6 (Ph)	**$[(4K)_2{\cdot}THF]_\infty$**	20
		18-crown-6 THF	SSIP	8	–	**$[K{\cdot}18\text{-}c\text{-}6{\cdot}2THF]^+[4]^-$**	10e
		15-crown-5	SSIP	10	–	**$[K{\cdot}(15\text{-}c\text{-}5)_2]^+[4]^-$**	10e
		2,2,2-crypt	SSIP	8	–	**$[K{\cdot}2,2,2\text{-}crypt]^+[4]^-$**	10e
$(C_6H_4)_2CH$ (**5**)	Li	–	Dimer	–	η^6 (Ph)	**$[5Li]_2$**	12
		EDA	Polymer	3	–	**$[5Li{\cdot}2EDA]_\infty$**	23
		DG	SSIP	6	–	**$[Li{\cdot}2DG]^+[5]^-$**	10c
		QN	Monomer	2	η^3 (C_α-C_i-C_o)	**5Li·2QN**	15
		Et_2O	Monomer	2	η^2 (C_α-C_i)	**$5Li{\cdot}2OEt_2$**	14
		Et_2O	Polymer	1	η^3, η^3 (C_i-C_α-$C_{i'}$)	**$[5Li{\cdot}OEt_2]_\infty$**	19
		THF	SSIP	4	–	**$[Li{\cdot}4THF]^+[5]^-$**	10d
	Na	–	Polymer	– (M1) – (M2)	$\eta^1(C_\alpha)$, $\eta^1(C_\alpha)$, $\eta^1(C_\alpha)$ η^4 (C_m-C_o-C_i-$C_{o'}$), η^4 (C_m-C_o-C_i-$C_{o'}$), η^4 (C_m-C_o-C_i-$C_{o'}$)	**$[5Na]_\infty$**	13
		DG	Dimer	4	$\eta^1(C_\alpha)$	**$[5Na{\cdot}DG]_2$**	10c
		DG	SSIP	6	–	**$[Na{\cdot}2DG]^+[5]^-$**	10c
		PMDETA	Monomer	3	η^5 (Cp)	**5Na·PMDETA**	16
		TMEDA	Polymer	2	$\eta^1(C_\alpha)$, η^3 (C_i-C_α-C_i)	**$[5Na{\cdot}TMEDA]_\infty$**	16
		TMPDA	Tetramer	2 (M1) 2 (M2)	$\eta^1(C_\alpha)$, η^3 (C_i-C_α-C_i) η^5 (Cp), η^2 (C_o-C_m)	**$[5Na{\cdot}TMPDA]_4$**	16
	K	THF	Polymer	1	η^2 (C_α-C_i), η^4 (C_o-C_m-C_p-$C_{m'}$), η^6 (Ph)	**$[(5K)_2{\cdot}THF]_\infty$**	13
		DG	Polymer	3 (M1) 1 (M2)	η^6 (Ph), η^6 (Ph) η^6 (Ph), η^2 (C_m-C_p), η^5 (Cp)	**$[(5K)_2{\cdot}DG]_\infty$**	10c
		DG	Trimer	3	η^5 (Cp), η^2 (C_α-C_i)	**$[5K{\cdot}DG]_3$**	10c
		18-crown-6	Monomer	6	η^6 (Ph)	**5K·18-c-6**	10b
		18-crown-6 THF	SSIP	8	–	**$[K{\cdot}18\text{-}c\text{-}6{\cdot}2THF]^+[5]^-$**	11
		18-crown-6 DME	Dinuclear	7	η^6 (Ph)	**$[5K{\cdot}18\text{-}c\text{-}6]_2{\cdot}DME$**	10b
		18-crown-6 THF	Dinuclear	7	η^6 (Ph)	**$[5K{\cdot}18\text{-}c\text{-}6]_2{\cdot}THF$**	10b
		18-crown-6 Pyridine	Dinuclear	7	η^3 (C_i-C_o-C_m)	**$[5K{\cdot}18\text{-}c\text{-}6]_2{\cdot}py$**	11
		TMEDA	Polymer	2	η^5 (Cp), η^3 (C_i-C_α-$C_{i'}$)	**$[5K{\cdot}TMEDA]_\infty$**	21
		TMEDA	Monomer	4	η^5 (Cp)	**5K·2TMEDA**	17
		PMDETA	Polymer	3	η^5 (Cp), $\eta^1(C_\alpha)$	**$[5K{\cdot}PMDETA]_\infty$**	22
2-PyCHPh (**6**)	Li	TMEDA	Dimer	2	η^1 (N)	**$[6Li{\cdot}TMEDA]_2$**	24

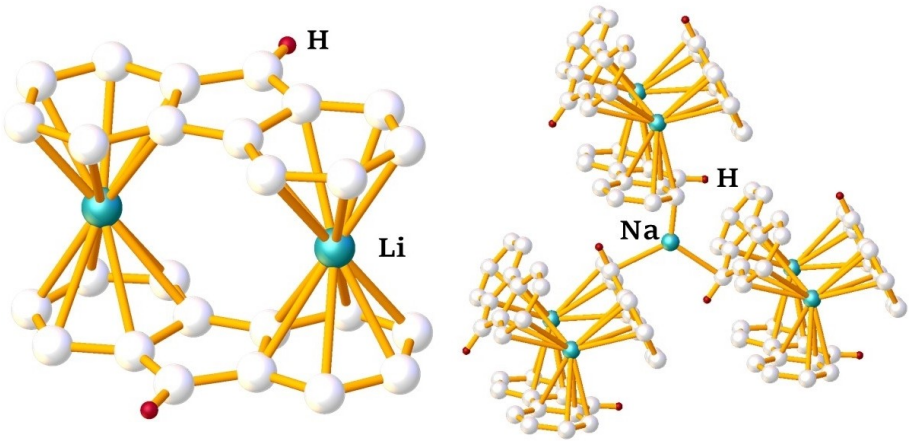

Figure 3. Molecular structure of unsolvated fluorenyllithium (left) and section of the polymeric structure of unsolvated fluorenylsodium (right).

If sufficient steric bulk is provided, monomeric complexes can be realised. Lithium binds to the fluorenyl anion in a η^2 or η^3 fashion when solvated by two diethyl ether ligands (**5Li·2OEt$_2$**)[14] or quinuclidine (**5Li·2QN**)[15] respectively, while sodium and potassium prefers a η^5 arrangement to the central ring in **5Na·PMDETA**[16] (Figure 4) or **5K·2TMEDA** (PMDETA = *N*,*N*,*N*′,*N*″,*N*″-pentamethyldiethylenetriamine; TMEDA = *N*,*N*,*N*′,*N*′-tetramethylethylenediamine).[17] Despite the diphenylmethyl anion not having the central 5-membered ring, it still uses the same five carbon atoms to coordinate to Na in monomeric **4Na·PMDETA** (Figure 4).[18]

Cyclo-oligomers are rare and often involve at least partial departure from η^5 coordination to help alleviate steric pressure. For example, diglyme solvated fluorenylsodium forms a dimer, **[5Na·DG]$_2$**,[10c] with the central oxygen atom of each diglyme molecule bridging the two sodium cations giving a η^2/η^2 type coordination and resulting in a central Na_2O_2 ring. The anions then bind to Na in a η^1 fashion via C_α (Figure 5). The almost perpendicular nature of the fluorenyl ring to sodium [Na–C–C angles of 84.9(1)° and 92.5(1)°] opens the possibility of a η^3 interpretation but the extended bond lengths to the adjacent carbon atoms ultimately preclude this. Moving to potassium results in cyclotrimeric **[5K·DG]$_3$** (Figure 5).[10c] Each cation bridges two separate fluorenyl anions, coordinating η^5 to one and η^3 to the other fluorenyl anion, and completes its coordination via a tridentate diglyme ligand.

Diphenylmethylsodium·TMEDA and fluorenylsodium·TMPDA both crystallize as cyclotetramers, with two distinct Na environments, despite the Lewis donors coordinating in a bidentate fashion each time. In **[4Na·TMEDA]$_4$**,[18] the first sodium (Na1, Figure 6) is bonded to the C_α of two diphenylmethyl anions. In contrast, Na2 is bonded to one C_α of a diphenylmethyl anion (ligand B) whilst also bonded to the *ortho* and *meta* ring positions of another diphenylmethyl anion (ligand A), evidenced by the large increase in Na–C(H) distance from about 2.7 to over 4 Å. In **[5Na·TMPDA]$_4$**[16] Na1 shows η^3/η^1 bonding to Cp ring of two anions while the second Na cation displays η^5 binding to the central ring of one fluorenyl anion (ligand A) but η^2 to the peripheral edge of one fused phenyl ring (ligand B) (Figure 6).

Both diphenylmethyl and fluorenyl complexes can polymerize if insufficient Lewis donors are present. For example, with

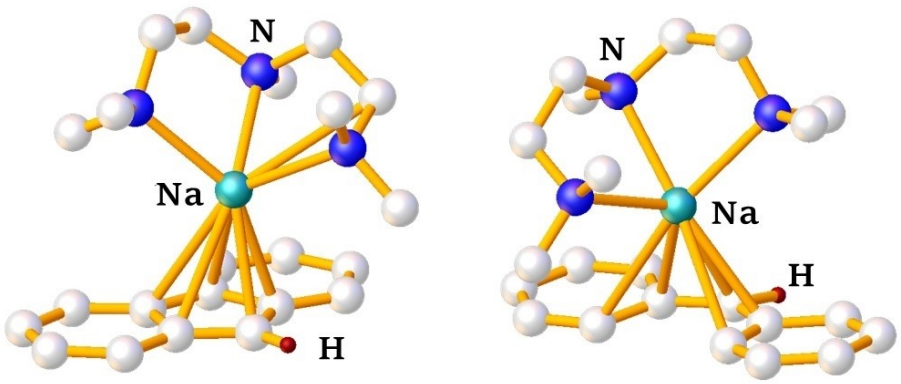

Figure 4. η^5 Coordination of Na·PMDETA to fluorenyl anion (left) and diphenylmethyl anion (right).

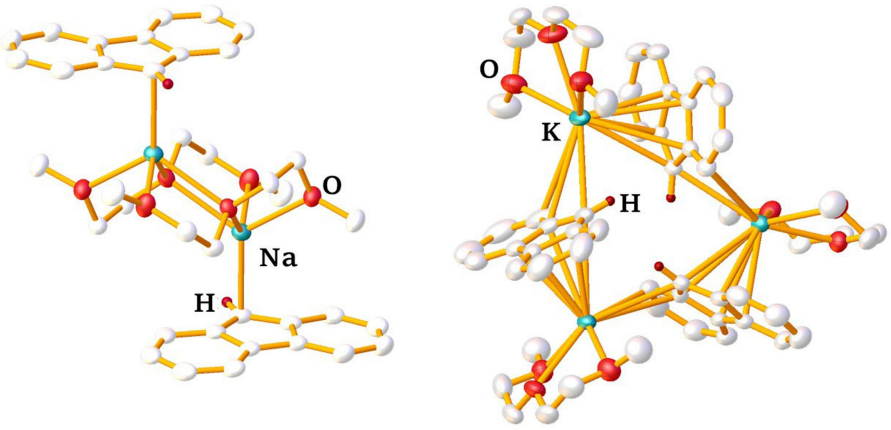

Figure 5. Molecular structures of diglyme solvated fluorenyl cyclo-oligomers **[5Na·DG]$_2$** (left) and **[5K·DG]$_3$** (right).

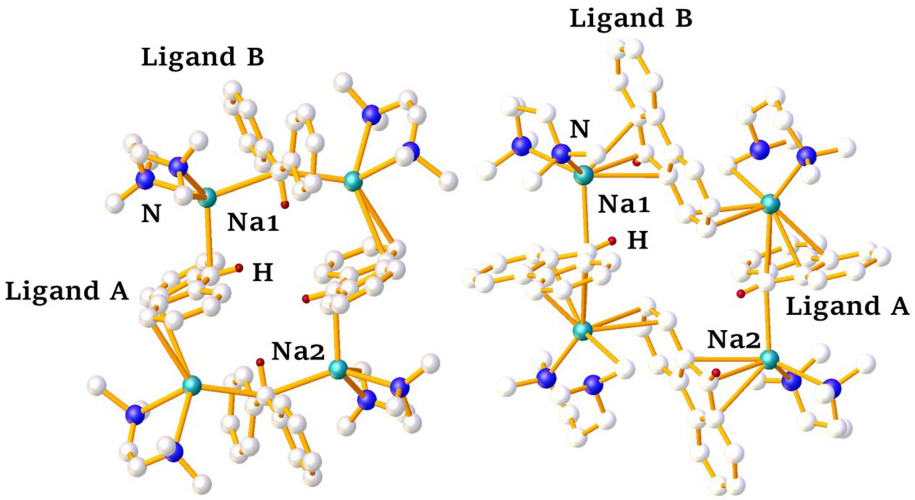

Figure 6. Molecular structures of cyclotetramers **[4Na·TMEDA]$_4$** (left) and **[5Na·TMPDA]$_4$** (right).

sub-stoichiometric diethyl ether fluorenyllithium polymerizes in **[5Li·OEt$_2$]$_\infty$**,[19] *viz-a-viz* the doubly-solvated derivative which is monomeric. Likewise, lowering the stoichiometry of diglyme present with fluorenylpotassium yields polymeric **[(5K)$_2$·DG]$_\infty$**[10c] rather than the trimer delivered with a 1:1 ratio (see above). A stoichiometric deficit of THF leads both diphenylmethylpotassium and fluorenylpotassium to polymerize with THF bridging adjacent K centres in **[(4K)$_2$·THF]$_\infty$**[20] and **[(5K)$_2$·THF]$_\infty$**[13] respectively. In the presence of TMEDA, fluorenylsodium and fluorenylpotassium both polymerize, with the metal-anion interactions reflective of the size of the metal. In **[5Na·TMEDA]$_\infty$**,[16] Na bridges two anions in a η^1/η^3 fashion; whereas potassium in **[5K·TMEDA]$_\infty$** utilizes a η^3/η^5 bridging motif.[21] Increasing the denticity via PMDETA in **[5K·PMDETA]$_\infty$** does not prevent polymerization but enforces a change in coordination to η^1/η^5.[22] The final polymeric structure of note is that of fluorenyllithium·ethylenediamine (**[5Li·2EDA]$_\infty$**, Figure 7), where Li cations are solvated by three N atoms from different EDA ligands, which each bridge to another Li cation

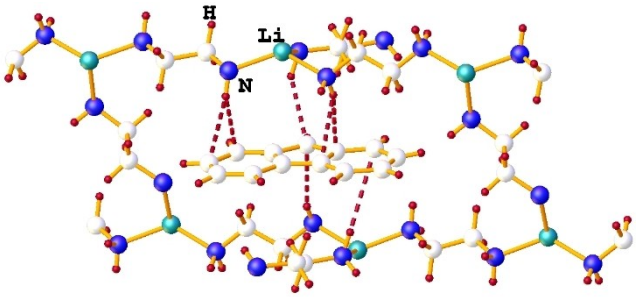

Figure 7. Section of polymeric structure of **[5Li·2EDA]$_\infty$** showing fluorenyl anion encapsulated within hydrogen bonded network.

resulting in a polymeric network of cations.[23] No interactions exist between the lithium cations and fluorenyl anions evidenced by the shortest separation distance of 4.03 Å, though there is a network of hydrogen bonding interactions between the amine H atoms of the EDA donor and fluorenyl carbons

demonstrated by N···C separation of less than 2.80 Å in the N–H···C units.

Crystallographically characterized 2- and (4-pyridyl)(phenyl)methyl structures are scarce, increasing the novelty of those disclosed within our results (see below). To our knowledge, the only reported example of an alkali-metal complex of 2-benzylpyridine is the TMEDA solvated lithium dimer, **[6Li·TMEDA]$_2$** (Figure 8).[24] Its distorted tetrahedral Li cations bridge the N atoms of the two anions, which are in the amide conformation, resulting in a 4-atom Li_2N_2 ring. There is no interaction between Li and the pendant Ph groups.

Hitherto, there have been no reports of alkali-metal phenyl(4-pyridyl)methyl structures. Notably 4-benzylpyridine acts as a neutral Lewis donor to lithium in **LiBH$_4$·(7H)$_3$**.[25] Here Li is coordinated by the N atoms of three 4-benzylpyridine groups and by three hydrides of a BH_4 anion, with the sp^3 nature of the bridging carbon evident in part by the non-planar nature of the two six-membered rings.

Results and discussion

Synthesis and characterization of monomeric alkali-metal diphenylmethyl complexes

We commenced our study of monomeric alkali-metal diphenylmethyl (**4**) complexes by attempting to deprotonate diphenylmethane with *n*BuLi in hexane solvent. While more acidic than toluene, diphenylmethane is still not sufficiently acidic for this reaction to proceed. However, upon adding Me_6TREN (tris[2-(dimethylamino)ethyl]amine), a tetrafunctional donor used previously by us to prevent oligomerization of alkali-metal complexes, a reaction occurred giving a red precipitate, due to the Lewis donor deaggregating the base and thus enhancing its basicity. Though the precipitate re-dissolved on adding warm THF, upon cooling a red oil separated rather than crystalline material. On repeating the reaction with PMDETA, the resulting orange crystals were confirmed by XRD as the desired monomeric complex Ph_2CHLi·PMDETA (**4Li·PMDETA**, Figure 9). To our knowledge, this complex represents the first example of a contacted diphenylmethyllithium complex, with the only related example a solvent-separated variant with Li sequestered by two 12-crown-4 ligands, **[Li·(12-c-4)$_2$]$^+$[4]$^-$**.[10a]

To realise monomeric heavier alkali-metal diphenylmethyl complexes, a Lochmann-Schlosser superbase approach[26] was taken where *n*BuLi was added to diphenylmethane in hexane and combined with a metal *tert*-butoxide (MO*t*Bu; M = Na or K), yielding **4Na·Me$_6$TREN** and **4K·Me$_6$TREN** respectively (Figure 10). The structure of the potassium complex was heavily disordered but confirmed unequivocally isostructural connectivity to **4Na·Me$_6$TREN** (see table 2 for selected bond parameters).

The coordination of the formally carbanionic centre in **4Li·PMDETA** is best described as distorted trigonal pyramidal. Li is positioned at the apex, and the CH^- bridge is in the centre of the base with *ipso* carbons surrounding it in the plane. The Li–C–H angle in **4Li·PMDETA** [86.9(1)°, note the hydrogen atom was located and refined] is distorted from that in a perfect trigonal pyramidal structure (90°) and the angles in the base of the pyramid total 356.4°. The ratio of the Li–C_{ipso}: Li–CH bond lengths provides supplemental evidence of the Li location in relation to the benzyl ring. This gives an idea of the hybridisation at the carbanionic carbon and hence the degree of charge delocalisation over the anion. These ratios for both *ipso* carbons in **4Li·PMDETA** (1.300 and 1.258) are slightly larger than that of the related benzyl complex **1Li·PMDETA** ($PhCH_2Li$·PMDETA; 1.222 and 1.193 for the two independent molecules).[27] This indicates that the Li cation in **4Li·PMDETA** is more strongly bound to the C_α atom when compared to a structure with only one aromatic ring (**1Li·PMDETA**) and suggests lesser delocalisation of negative charge from the

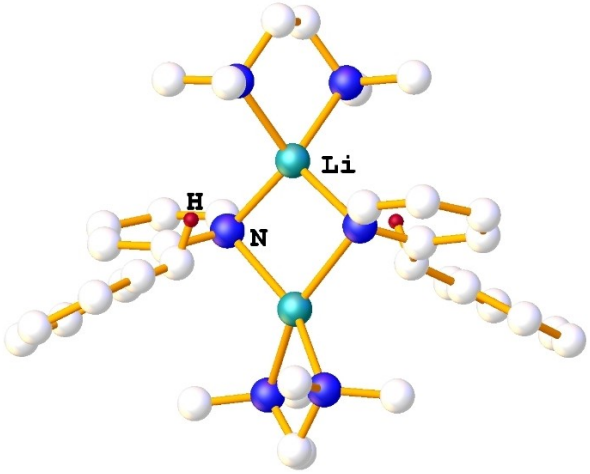

Figure 8. Molecular structure of lithium (2-pyridyl)(phenyl)methyl complex **[6Li·TMEDA]$_2$**.

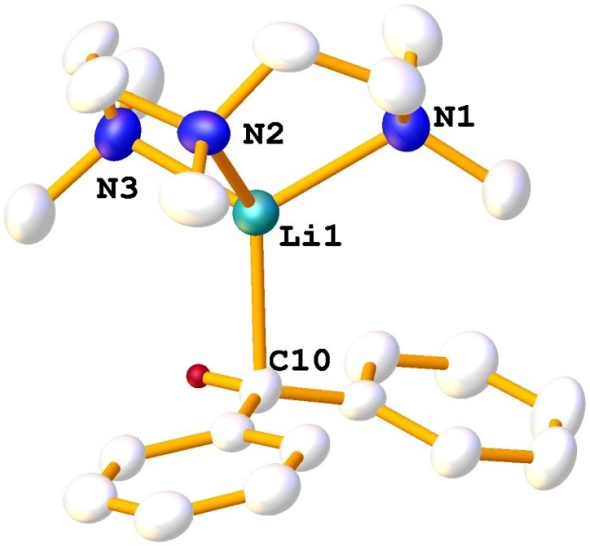

Figure 9. Molecular structure of one independent molecule of **4Li·PMDETA** with H atoms (except on metallated carbon atom) omitted for clarity and with thermal ellipsoids at 50% probability.

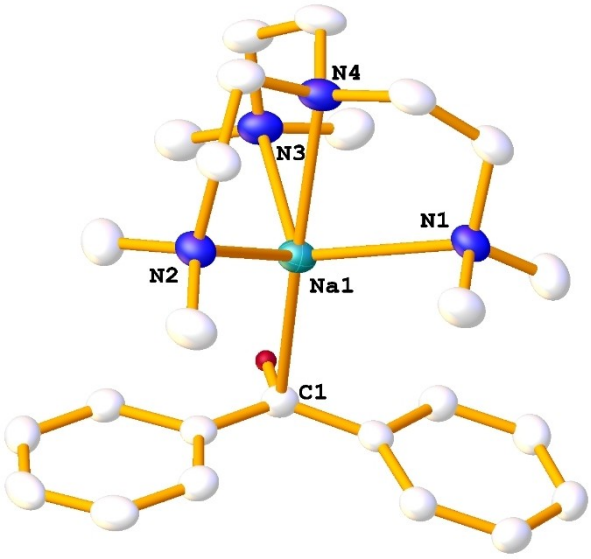

Figure 10. Molecular structure of **4Na·Me$_6$TREN** with H atoms (except on metallated carbon atom) omitted for clarity and with thermal ellipsoids at 50% probability. Note **4K·Me$_6$TREN** is isostructural.

carbon bridge into the aromatic rings. This is further evidenced by the Li–CH–C_{ipso} angles, which in **4Li·PMDETA** [97.7(3)° and 102.8(3)°] are larger than those in the benzyllithium complex [90.8(2) and 93.9(2)°]. This suggests greater sp^3 character at the formally anionic C atom of **4Li·PMDETA** and that the single negative charge is less delocalised, thus diminishing the charge density at any one ring and hence, reducing the strength of the alkali-metal and aromatic ring interaction. We note here that the bulkier higher dentate donor Me$_6$TREN results in greater sp^3 character in **1Li·Me$_6$TREN** than in **4Li·PMDETA** [Li–CH–C_{ipso} angles = 133.4(2)/126.4(1)° for the two independent molecules][9a] demonstrating that the bulk of the Lewis donor can affect the apparent hybridization at the anionic carbon centre (note each benzyl complex displays a similar $^1J(^{13}C–^1H)$ coupling constant – 132 and 134 Hz – which suggests both have greater sp^3 character than diphenylmethyl complex **4Li** in the solution state, see below). Though **4Na·Me$_6$TREN** and **4K·Me$_6$TREN** have monomeric structures comparable to that of **4Li·PMDETA**, due to the difference in donor, the sodium and potassium complexes have a formally five-coordinate metal centre. **4Na·Me$_6$TREN** has a similar distorted trigonal pyramidal geometry at the deprotonated C to that of **4Li·PMDETA** with the M–C–H angle this time significantly larger than the ideal angle of 90° [97.2(1)°] potentially as a consequence of the steric clashing by the additional donor arm present, having changed from tridentate PMDETA to tetradentate Me$_6$TREN. Also, the angles in the plane of the bridging carbon are close to the ideal of 360° at 358.4°. The Na–C distance involving the central C atom (2.747(2) Å) in **4Na·Me$_6$TREN** is similar to those of the corresponding bonds in ([**4Na·TMEDA**]$_4$ and **4Na·PMDETA**) despite each having a different donor ligand. All three complexes display similar benzyl geometries demonstrated by the equivalence of the C_{ipso}–C–C_{ipso} angle in each anion (**4Na·Me$_6$TREN** and [**4Na·TMEDA**]$_4$ = 131°, **4Na·PMDETA** = 132°). The Ph rings in both the Me$_6$TREN and PMDETA monomers are close to coplanar (**4Na·Me$_6$TREN** = 18.9(5)°, **4Na·PMDETA** = 4.3(2) and 7.7(2)°), hinting that the negative charge is delocalised away from the formally carbanionic centre. DFT calculations show a considerable increase in the phenyl ring rotation barrier on moving from **4H** (0.4 kcal mol^{-1}) to the free **4**$^-$ anion, **4Na·PMDETA** or **4Na·Me$_6$TREN** (13.3, 10.0 and 11.0 kcal mol^{-1} respectively, see Figure S39), supporting charge delocalisation although the tilt angle in gas-phase monomeric **4Na·Me$_6$TREN** is slightly larger at 25.5°, suggesting crystal packing effects may also contribute slightly here. In addition to this, the M–C_{ipso} bond lengths in monomeric **4Na·Me$_6$TREN** and **4Na·PMDETA** (all approximately 2.8–2.9 Å) are shorter than those of the polymeric TMEDA structure (3–4 Å). The Na–C–C_{ipso} angles of **4Na·Me$_6$TREN** [85.5(1) and 100.5(1) Å] are smaller than those in the Li complex, showing a very slight migration of the Na cation towards the aromatic systems, and the disparity in the two values demonstrates a clear preference for one ring over the other. While the molecular structure of **4K·Me$_6$TREN** displays too much disorder to allow any discussion of the bonding parameters, it is clear that the potassium centre has not moved to a position which could be considered as η^6 coordinated to the aromatic ring, as is seen in monomeric potassium benzyl-type complexes, with any migration com-

Table 2. Selected experimental bond parameters (Å and °) for diphenylmethyl (**4**) and fluorenyl (**5**) complexes.

	4Li·PMDETA	4Na·Me$_6$TREN	5Na·Me$_6$TREN	5K·Me$_6$TREN
M–C_α	2.247(9)	2.747(2)	2.954(1)	3.064(3)
M–C_{ipso}(1)	2.921(9)	3.317(2)	2.850(1)	3.020(3)
M–C_{ipso}(2)	2.826(9)	2.994(2)	3.496(1)	3.128(3)
M–N_{cent}	2.146(9)	2.517(2)	2.578(1)	2.926(2)
M–NMe_2	2.122(8)	2.634(2)	2.605(1)	2.812(2)
M–NMe_2	2.166(9)	2.548(1)	2.514(1)	2.771(3)
M–NMe_2	–	2.544(2)	2.515(1)	2.805(3)
C_α–C_{ipso}(1)	1.434(6)	1.426(2)	1.410(1)	1.419(4)
C_α–C_{ipso}(2)	1.439(7)	1.426(2)	1.419(1)	1.401(4)
M–C_α–C_{ipso}(1)	102.8(3)	100.5(1)	71.84(7)	74.8(2)
M–C_α–C_{ipso}(2)	97.7(3)	85.5(1)	100.17(7)	79.5(2)
C_{ipso}(1)–C_α–C_{ipso}(2)	127.7(4)	131.1(1)	107.5(1)	107.2(3)
C_o–C_{ipso}(1)–$C_{o'}$	114.0(4)	114.0(1)		
C_o–C_{ipso}(2)–$C_{o'}$	114.9(5)	114.1(1)		

pared to the lithium and sodium complexes only negligible. Crystal structure data of each complex was complemented in solution by ^{1}H and ^{13}C NMR spectra in d_8-THF (table 3; Figures S1–S7), as the complexes were not sufficiently soluble in C_6D_6.

The ^{1}H NMR spectra of diphenylmethyl complexes **4** (table 3), which each contained a minor amount (16–37%) of parent diphenylmethane which could not be removed under vacuum (b.p. = 264 °C), confirm metallation of diphenylmethane as the CH_2 bridge resonance has a reduced integration from 2 to 1 upon deprotonation to Ph_2CH^-. The corresponding chemical shift also moves downfield slightly as cation size increases (4.12, 4.24 and 4.31 ppm for Li, Na and K respectively) compared to that in the protonated substrate (3.94 ppm). However, this downfield movement is less pronounced than in the benzyl series **1** (2.08, 2.51 and 3.21 ppm respectively) illustrating the diminished movement of the cation in the diphenylmethyl series as evidenced also in the molecular structures. Aromatic resonances are moderately upfield shifted but are similar for all three complexes, again in contrast to the benzyl family of complexes (**1**) where the upfield shift of the *para* resonance increases with metal size (and hence metal-ring interaction) from 7.05 (M = H) to 6.23/5.93/5.24 ppm for Li/Na/K respectively. Both rings within each complex display the same aromatic shifts suggesting that they are the same or are exchanging when in solution, which contrasts with the crystal structure where one ring sits slightly closer to the metal than the other. This suggests that in solution the metal cation is lying equidistant between the rings, or alternatively, is moving between the two. Finally, the $^{1}J(^{13}C–^{1}H)$ coupling constants for the bridging CH^- resonance can be used to provide additional evidence about the delocalisation of negative charge. Boche et al. showed the coupling constant for a pyramidalised sp^3 benzyl carbanion is expected to be 125 Hz, while the expected value for a planar sp^2 benzyl carbanion (that is with the negative charge completely delocalised into the ring) is 167 Hz.[28] Complexes **4Li·PMDETA**, **4Na·Me$_6$TREN** and **4K·Me$_6$TREN** display similar coupling constants of 142, 145 and 146 Hz respectively. This suggests that in solution the bridging C in each complex has a hybridisation between these two extremes. These three complexes having similar values indicate that the metal-ligand interaction changes only marginally as a function of alkali-metal in solution, closely mirroring the solid-state structures described earlier.

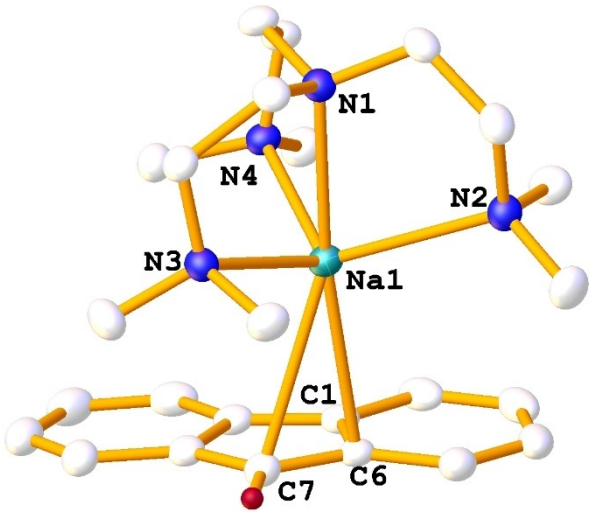

Figure 11. Molecular structure of **5Na·Me$_6$TREN** with H atoms (except on metallated carbon atom) omitted for clarity and thermal ellipsoids drawn at 50% probability.

Synthesis and characterization of monomeric alkali-metal fluorenyl complexes

Next, we decided to probe fluorene where the *ortho* C atoms on each ring are tethered together, which enforces greater planarity in the ligand and introduces a third aromatic ring upon deprotonation in a central substituted Cp ring. The synthetic procedure mirrored that of the diphenylmethyl complexes and yielded isolable monomeric complexes in each case. While the Li complex solvated by PMDETA (**5Li·PMDETA**) did not provide single crystals suitable for X-ray diffraction, the heavier complexes, both Me_6TREN solvated, were crystallographically characterised (**5Na·Me$_6$TREN** and **5K·Me$_6$TREN**).

Though **5Na·Me$_6$TREN** and **5K·Me$_6$TREN** (Figures 11 and 12 respectively, see table 2 for selected bond parameters) are monomers where the metal cation is η^4-coordinated by the Me_6TREN donor ligand, each cation engages differently with the planar fluorenyl anion. The Na complex has a η^2 bonding mode to it via the deprotonated C atom and an adjacent (*ipso*) C, in contrast to the η^5 arrangement of PMDETA monomer **5Na·PMDETA**,[16] reflecting the greater bulk of the tetradentate donor. This is supported by the Na–C bond lengths as in **5Na·Me$_6$TREN** the asymmetry of the metal ligand bonding is

Table 3. Selected NMR chemical shift data (ppm) for diphenylmethane and diphenylmethyl complexes in d_8-THF at 23 °C.

	Diphenylmethane		4Li·PMDETA		4Na·Me$_6$TREN		4K·Me$_6$TREN	
	^{1}H	^{13}C	^{1}H	^{13}C	^{1}H	^{13}C	^{1}H	^{13}C
ortho/meta	7.17	127.6	6.58	126.9	6.61	129.2	6.59	128.8
		128.2		116.5		117.7	6.51	116.8
para		125.2	5.72	106.7	5.74	108.7	5.70	107.5
CH^-	3.94 [a]	41.1[a]	4.12	73.4	4.24	75.3	4.31	79.4
ipso	–	140.8	–	146.6	–	147.3	–	146.2
$^{1}J(^{13}C–^{1}H)$ (Hz)	125		142		145		146	

[a] CH_2.

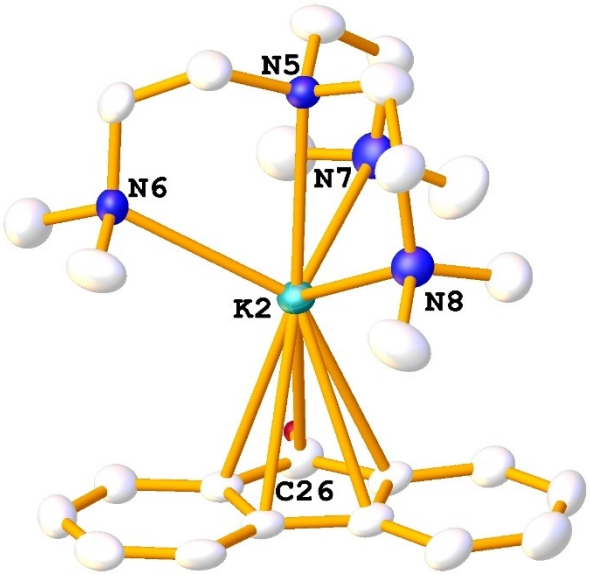

Figure 12. Molecular structure of one independent molecule of **5K·Me$_6$TREN** with H atoms (except on metallated carbon atom) omitted for clarity and thermal ellipsoids drawn at 50% probability.

more pronounced with Na–C_{ipso} bond distances of 2.850(1) and 3.496(1) Å; cf. 2.71 and 2.83 Å in **5Na·PMDETA**. This bonding mode is in contrast to that of **5K·Me$_6$TREN** where the metal occupies a centroid η^5 position above the 5-membered ring (Figure S33 for comparison). This is similar to the aforementioned PMDETA polymer **[5K·PMDETA]**$_\infty$, with the key difference that the presence of the additional *N*-donor is sufficient to prevent the η^1 interaction which propagates the infinite chain. This η^5 coordination mode is further supported by the relatively narrow range [3.020(3)–3.145(3) Å] in the bond lengths between K and all five C ring atoms. This range is narrower than those in other η^5 fluorenyl-potassium interactions [for example, 3.089(3)–3.302(3) Å in the PMDETA-solvated polymer;[22] 3.069(2)–3.318(2) Å in the diglyme-solvated trimer;[10c] and 3.071(5)–3.320(4) Å in the bis-TMEDA-solvated monomer.[17]

All three fluorenyl complexes were sufficiently soluble in C_6D_6 for their ^{1}H NMR spectra to be recorded (table 4, Figures S8–S14), although the lithium complex gave a particularly weak spectrum so its ^{13}C NMR spectrum was recorded in d_8-THF.

Similar to those of the diphenylmethyl complexes, the ^{1}H NMR spectra of the fluorenyl complexes evidence metallation through a downfield shift of the CH$^-$ proton although the shift is more noticeable in the fluorenyl complexes (from 3.49 to 5.97, 6.32 and 6.60 ppm for Li, Na and K respectively, table 4) due to the aromatic character gained by the CH group. This spread of chemical shifts is wider than that in the unsubstituted alkali-metal Cp(M) family of complexes (Cp=$C_5H_5^-$; M=Li–Cs), where the corresponding resonance in THF lies in the range 5.55–5.72 ppm,[29] demonstrating the ability of the fused Ph rings in the fluorenyl anion to modulate the location of the negative charge and hence the position/hapticity of the metal with respect to an unsubstituted Cp ring. The aromatic nature of the anions is further supported by the $^1J(^{13}C–^1H)$ coupling constants for CH$^-$, which are similar for **5Li·PMDETA** and **5Na·Me$_6$TREN** (about 158 Hz) and are indicative of sp^2 hybridization, suggesting the electronic nature of the fluorenyl ligand is much less dependent on the identity of the alkali-metal and is dictated by the aromatization afforded it upon deprotonation.

Synthesis and characterization of monomeric alkali-metal phenyl(2-pyridyl)methyl complexes

Next, a derivative of the diphenylmethyl ligand with a Lewis basic heteroatom was considered in 2-benzylpyridine (**6H**). The resulting anion can be regarded as a hybrid ligand between the diphenylmethyl ligand **4** and the previously studied 2-picolyl ligand. This study would determine whether the negative charge at the CH$^-$ bridge would rather remain localised at the bridgehead (carbanionic), be delocalised into the Ph ring like the benzyl complexes studied previously, or be delocalized into the pyridyl ring (aza-allyl) where it can potentially re-localise onto the nitrogen to give an enamido type ligand (Figure 1, bottom). Between ourselves and Stalke, all three examples have been crystallographically identified for 2-picolyllithium (Figure 13),[9c,30] dependent upon the Lewis donor solvating the Li cation, demonstrating the inherent flexibility/complexity in this ligand type.

Stalke has also studied the alkali-metal complexes of the related diphenyl(2-pyridyl)methyl ligand, Ph_2(2-Py)C$^-$ (**8**), acquiring a family of monomers in **8Li·2OEt$_2$**, **8Na·3THF** and **8K·PMDETA·THF**.[31] This ligand contains an additional Ph ring at the bridgehead as opposed to a H atom and thus has no option but to have one Ph ring in close proximity to the alkali-metal.

Table 4. Selected ^{1}H NMR chemical shift data (ppm) for fluorene and fluorenyl complexes in C_6D_6 at 23 °C.

	Fluorene	5Li·PMDETA	5Na·Me$_6$TREN	5K·Me$_6$TREN
ortho	7.27	7.73	7.78	7.86
meta	7.24	7.53	7.38	7.37
para	7.16	7.26	7.07	7.02
meta′	7.64	8.59	8.43	8.35
CH	3.49[a]	5.97	6.33	6.60
$^1J(^{13}C–^1H)$ (Hz)	130.9	158.6 [b]	158.4	–[c]

[a] CH_2 [b] taken from THF solution as C_6D_6 solution was too dilute to see $^{13}C–^1H$ coupling [c] too broad to resolve $^{13}C–^1H$ coupling, even at 65 °C.

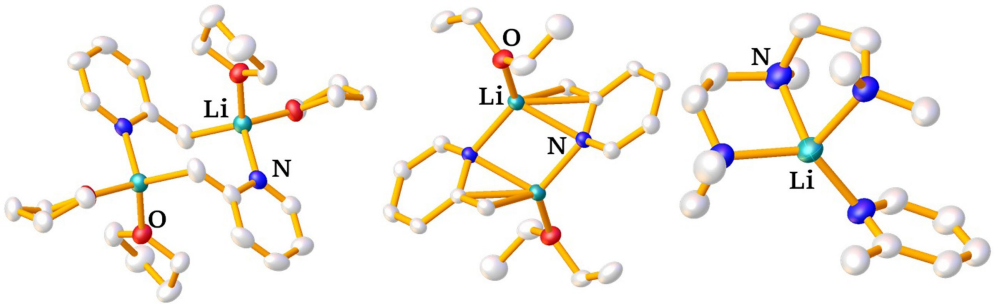

Figure 13. Previously reported molecular structures of **[2Li·2THF]$_2$** (carbanionic, left), **[2Li·OEt$_2$]$_2$** (aza-allyl, middle) and **2Li·PMDETA** (enamido, right)

The same synthetic protocol as employed previously, using 2-benzylpyridine (**6H**) as a substrate delivered crystalline material in all three cases. Unfortunately, only the data of the sodium complex, **6Na·Me$_6$TREN**, were of sufficient quality to discuss in detail. Preliminary data were too weak (**6Li·Me$_6$TREN**) or the structure was heavily disordered (**6K·Me$_6$TREN**), supporting only their connectivity; specifically that they are monomeric, the metal drifts from outside the NC_4 unit to within it (Figures S34–S36) and the ligand maintains a *cis*-disposition as alluded to with regard to the Na complex (see below). Furthermore, it was obvious that the Me$_6$TREN ligand was ligating η^3 to the Li centre with one $CH_2CH_2NMe_2$ arm lying free, a coordination mode that has been seen previously for this Lewis donor on coordinating to lithium.[32] Repeating the synthesis using PMDETA as the donor gave an oil and so was not studied further. **6Na·Me$_6$TREN** adopts a monomeric structure in the crystal (Figure 14) with Me$_6$TREN binding via all four nitrogen atoms. The ligand adopts a *cis* conformation of the Ph group with respect to the pyridyl ring nitrogen and appears to be coordinated to the metal via that N atom and also potentially via the C_ω, CH, C_{ipso} and C_{ortho} unit although it is difficult to determine this unequivocally since some of these 'interactions' may simply be two atoms forced close to one another as a consequence of the ligand orientation. The Na–N bond [2.565(2) Å] is noticeably longer than in Stalke's complex **8Na·3THF** [2.414 Å], presumably as a consequence of the Lewis acidic metal being coordinated to four Lewis donors in the Me$_6$TREN complex but only three in the THF complex, and/or the longer distance advocates an additional Na–Ph interaction. The Na in our complex appears closer to the pyridyl end of the NC_4 unit [comprising C6, C1, C8 and C7 in Figure 14 with distances of 3.027(2), 3.048(2), 3.132(2) and 3.040(2) Å respectively] than in the THF solvate, whose corresponding distances are 3.341(7), 3.496(6), 3.067(7) and 2.859(8) Å respectively. Stalke's closest carbon atom, C_{ortho}, was described as being at such proximity as a result of steric hinderance. However, with no second Ph group in **6Na·Me$_6$TREN**, it is plausible that its Ph ring is held *cis* to the pyridyl N atom by a long-range Na–Ph interaction since if there was no such interaction present then the Ph ring could lie *trans* to the N atom, that is away from the metal (see DFT analysis section for more details). With respect to the bonding in the ligand itself, a similar bonding pattern is seen within the NC_5 ring and shortening of the bond to the

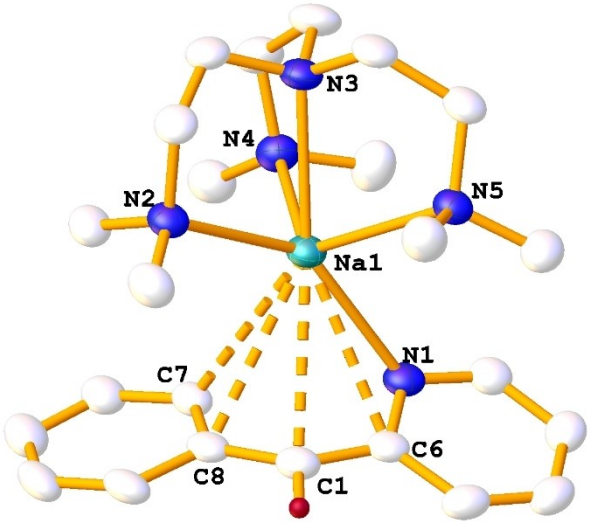

Figure 14. Molecular structure of **6Na·Me$_6$TREN** with H atoms (except on metallated carbon atom) omitted for clarity and thermal ellipsoids drawn at 50% probability. Selected bond lengths (Å) and angles (°): Na1–N1, 2.565(2); Na1–C6, 3.027(2); Na1–C1, 3.048(2); Na1–C8, 3.132(2); Na1–C7, 3.040(2); Na1–N2, 2.589(2); Na1–N3, 2.586(2); Na1–N4, 2.640(2); Na1–N5, 2.582(2); N1–Na1–N2, 144.34(6); N1–Na1–N3, 143.84(6); N1–Na1–N4, 95.36(6); N1–Na1–N5, 88.38(6); N2–Na1–N3, 71.10(6); N2–Na1–N4, 108.34(6); N2–Na1–N5, 103.82(6); N3–Na1–N4, 69.94(6); N3–Na1–N5, 70.63(6); N4–Na1–N5, 116.00(6).

bridgehead C atom as described by Stalke (Figure 15), suggesting that the negative charge is localised predominantly into the pyridyl ring, particularly at the nitrogen atom. The Na–N–C_{para} angle [134.06(9)°] is considerably deviated from the 180° expected for a neutral, Lewis donating pyridine coordinating to the metal centre, and is more akin to the nitrogen acting as a charged amide. In complex **4Na·Me$_6$TREN**, the data shows identical bond lengths for the bridging C to the C_{ipso} atoms [both 1.426(2) Å]; whereas in complex **6Na·Me$_6$TREN** the bond length between the CH^- and pyridyl C is slightly shorter [1.407(3) Å] than to the Ph ring [1.432(3) Å], suggesting a more conjugated single/double bond scenario. This is further supported by the bridging carbon appearing close to planarity [$\Sigma <= 358.0°$; note the H atom was located and refined]. The Ph ring maintains its aromatic character, albeit it with slightly

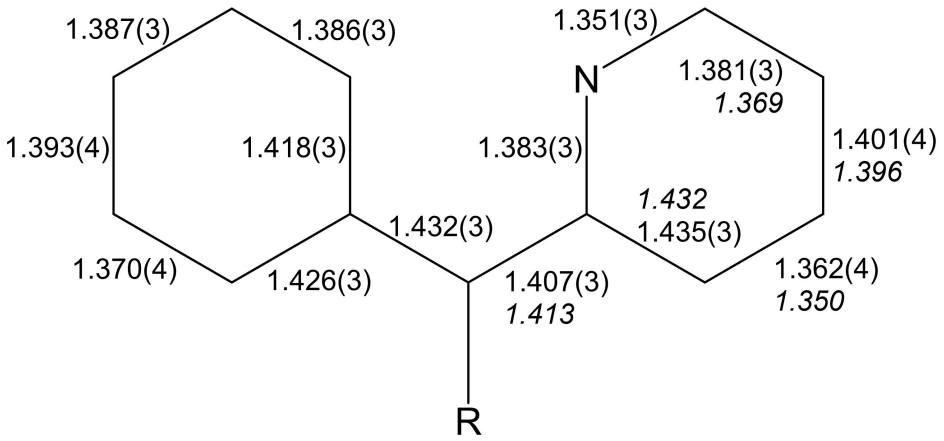

Figure 15. Bond lengths (Å) in phenyl(2-pyridyl)methyl anion of **6Na·Me$_6$TREN** (R=H) with selected average values for Ph$_2$(2-py)CM (M=Li, Na, K; R=Ph) in italics.

longer C_{ipso}–C_{ortho} bonds, presumably as a consequence of the interaction between the metal and C1/C8/C7.

These samples were also analysed in solution by ^{1}H and ^{13}C NMR spectroscopy in d_8-THF due to poor solubility in C_6D_6 (Figures S15–S22). The Li and K complexes contained some protonated benzylpyridine (b.p. 276 °C, 26 and 4% respectively) which did not interfere with the interpretation of the electronic structure of the complexes.

The ^{1}H NMR spectra of the three complexes (summarized in table 5) are essentially similar, suggesting a similar metal-ligand bonding pattern in each. In particular, the resonance for the H atom on the deprotonated carbon is deshielded and the heteroatomic ring resonances are all shielded with respect to the parent substrate suggesting loss of aromaticity and movement towards a conjugated bonding system. Further, the Ph *ortho*/*meta* CH units give only a single environment each, suggesting that the Ph ring is free to rotate in solution at room temperature since if the molecular structures were maintained then splitting and inequivalence of the *ortho*/*ortho*′ and *meta*/*meta*′ environments is likely to occur. The $^1J(^{13}C–^1H)$ coupling constants are similar, spanning a range of only 2 Hz, reflecting an intermediacy between sp^2 and sp^3 hybridization at the CH bridge. Two resonances which do stand out are the *ortho* CH and β′ CH resonances of the Li complex. The former is upfield shifted with respect to the protonated substrate as opposed to those of the Na/K complexes which see a downfield shift and the latter only moves to 6.65 ppm; whereas the heavier alkali-metal complexes are shifted considerably more, to 5.98/5.96 ppm respectively. Interestingly, a recollection of the ^{1}H NMR spectrum of **6Na·Me$_6$TREN** in d_8-THF at 233 K reveals a lower intensity duplicate set of resonances, indicative of an alternative isomer, in a 1:3 ratio with respect to the original isomer seen at room temperature (Figure S19). These changes were reversible with the spectrum reverting to the original upon re-recording at room temperature. This minor isomer sees the *ortho* and β′ resonances move in a way which now replicates the room temperature spectrum of **6Li·Me$_6$TREN**, suggesting the minor isomer of the sodium complex is the same as that of the major (only) isomer of the lithium complex. NOESY NMR spectroscopy was attempted on **6Na·Me$_6$TREN** to see if *cis*/*trans* isomers could be assigned since the *ortho* resonance should come into close proximity to the β′ resonance when the phenyl ring lies *cis* to the β′ position (*trans* to the ring N). However, this provided no further clarity, perhaps due to the broad nature of the resonances in question. Repeating at high temperature did not resolve these resonances further. No second isomer was witnessed for **6Li·Me$_6$TREN** or **6K·Me$_6$TREN** when the temperature was altered.

Table 5. Selected ^{1}H NMR chemical shift data (ppm) for 2-Benzylpyridine and phenyl(2-pyridyl)methyl complexes in d_8-THF at 23 °C.

	2-Benzylpyridine	6Li·Me$_6$TREN	6Na·Me$_6$TREN	6 K·Me$_6$TREN
ortho	7.08–7.14	6.80	7.32	7.39
meta	7.19–7.27	6.74	6.77	6.75
para	7.03	6.15	6.11	6.08
α	8.45	7.52	7.47	7.55
β	7.19–7.27	5.21	5.36	5.37
β′		6.65	5.99	5.96
γ	7.51	6.45	6.44	6.42
CH^-	4.08 [a]	4.45	4.42	4.45
$^1J(^{13}C–^1H)$ (Hz)	128	149	147	148

[a] CH_2.

Synthesis and characterization of monomeric alkali-metal phenyl(4-pyridyl)methyl complexes

Finally, we considered the substrate 4-benzylpyridine (**7H**) with the pyridyl heteroatom occupying the 4-position, which moves the CH_2Ph group *para* to the N and makes it less accessible to the metal if the negative charge is re-localized to the N upon deprotonation. Following the same protocol as described previously with **7H** as the substrate, we were only able to isolate a solid Me_6TREN solvated sodium complex (**7Na·Me$_6$TREN**), with the lithium and potassium complexes yielding oils. However, for the reactions involving PMDETA, recrystallization yielded solid complexes for all three alkali-metals, of which only the sodium complex, **7Na·PMDETA** yielded single crystals suitable for an X-ray structural determination. While the larger donor successfully traps the complex as a *N*-coordinated monomer, the tridentate donor results in a polymeric structure which includes *N*-coordination but also *C*-coordination of another ligand to the metal to complete the five-coordinate nature of the metal (Figure 16).

To our knowledge, these are the first crystal structures of the phenyl(4-pyridyl)methyl anion. The ligand binds to the metal solely through N in monomeric **7Na·Me$_6$TREN**, with the Na cation lying outside the plane of the pyridyl ring [Na1–N1–C_{para} 152.7(1)°] and a Na–N distance of 2.391(2) Å which is considerably shorter than that in **6Na·Me$_6$TREN** [2.565(2) Å] and is consistent with a sodium-secondary amide interaction.[33] The C_α–C_β bonds in the NC_5 ring (Figure 17) are noticeably shorter than the C_β–C_γ, as the C_γ–CH is shorter than the CH–C_{ipso} bond, suggesting a single bond/double bond conjugation. Collectively, this evidence is consistent with re-localization of the negative charge from the deprotonated C into the pyridyl ring and onto the nitrogen atom. The two 6-atom rings are almost coplanar with a tilt angle of 8.10(9)°.

The phenyl(4-pyridyl)methyl anion in polymeric **7Na·PMDETA** is remarkably similar to that in monomeric **7Na·Me$_6$TREN** (Figure 17), as are the N–Na distances [2.391(2) and 2.391(3) Å] suggesting a similar charge distribution. The rings are close to being coplanar in both cases at 6.8(1) and 8.1(1)° for the polymer and monomer, respectively. That said, the sodium atom in the polymer has moved approximately 10° closer to planarity with respect to the pyridyl ring at 162.6(1)° which could be due to greater neutrality at N or alternatively be an artefact of the fifth coordination site being a CH(Ph)(4-py) unit which is considerably bulkier than the $Me_2NCH_2CH_2$ arm of Me_6TREN. Furthermore, the geometry of the bridging carbon is very similar to that seen in the related diphenylmethyl complex **4Na·Me$_6$TREN** emphasised by the Na–C distance of this unit at 2.793(4) Å [2.747(2) Å] and the Na–CH–C angles which would suggest a similar degree of negative charge localized at this bridging carbon atom.

NMR spectra (table 6) of **7Li·PMDETA** and **7Na·Me$_6$TREN** were collected in C_6D_6 (Figures S23–S28). **7Na·PMDETA** and **7K·PMDETA** were insoluble in C_6D_6 and thus had their spectra collected in d_8-THF instead (Figures S29–S32), suggesting that the infinite aggregation in the sodium complex is unsurprisingly replicated in the potassium complex. The anion in the Li and Na complexes give similar C_6D_6 spectra, with the Ph groups appearing in the typical aromatic region, the pyridyl resonances moving upfield and the CH bridge moving downfield with respect to the protonated substrate 4-benzylpyridine, while the CH coupling constant increases by approximately 20 Hz.

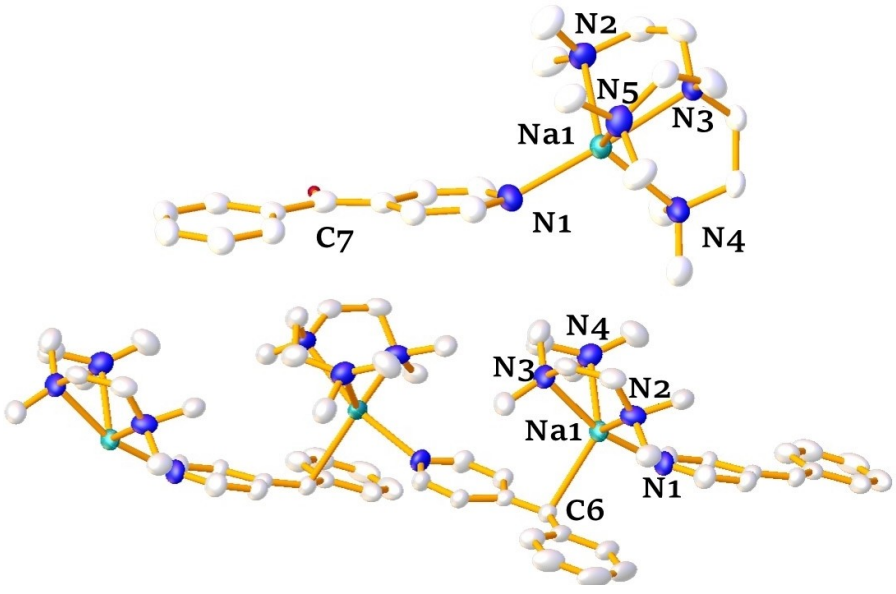

Figure 16. Molecular structure of **7Na·Me$_6$TREN** (top) and a dinuclear section of the **7Na·PMDETA** polymer (bottom) with H atoms (except on metallated carbon atom) and disordered component of Me_6TREN and PMDETA omitted for clarity, and with thermal ellipsoids at 50% probability. Bond parameters for **7Na·Me$_6$TREN** with those for **7Na·PMDETA** in parentheses (n.a. = data not applicable): Na1–N1, 2.391(2) [2.391(3)]; Na1–N2, 2.535(3) [2.525(3)]; Na1–N3, 2.493(2) [2.483(3)]; Na1–N4, 2.489(3) [2.634(3)]; Na1–N5, 2.465(2) [n.a.]; Na1–C6′, n.a. [2.793(3)]; N1–Na1–N2, 103.50(9) [102.16(10)]; N1–Na1–N3, 176.09(9) [163.47(10)]; N1–Na1–N4, 108.29(9) [96.87(10)]; N1–Na1–N5, 108.26(8) [n.a.]; N2–Na1–N3, 72.59(8) [73.67(9)]; N2–Na1–N4, 112.42(10) [113.52(10)]; N2–Na1–N5, 110.67(9) [n.a.]; N3–Na1–N4, 73.57(8) [71.15(10)]; N3–Na1–N5, 73.68(8) [n.a.]; N4–Na1–N5, 113.13(9) [n.a.].

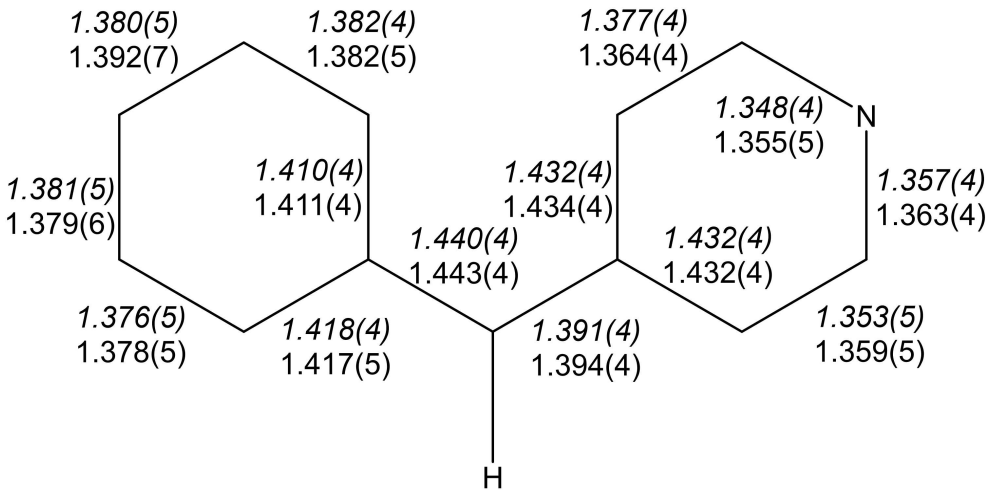

Figure 17. Bond lengths (Å) in the phenyl(4-pyridyl)methyl anion of **7Na·Me$_6$TREN** monomer (top value, in italics) and **7Na·PMDETA** (bottom value)

Table 6. Selected ^{1}H NMR chemical shift data (ppm) for 4-benzylpyridine and phenyl(4-pyridyl)methyl complexes in C_6D_6 at 23 °C.

	4-BnPy	7Li·PMDETA	7Na·Me$_6$TREN	4-BnPy[a]	7Na·PMDETA [a]	7K·PMDETA [a]
ortho	6.88	7.68	7.63	7.18	6.82	6.81
meta	7.08	7.37	7.35	7.26	6.75	6.76
para	7.08	6.84	6.80	7.17	6.17	6.15
α	8.46	6.98/6.84	7.21/7.02	8.41	6.97/6.80	7.10/6.91
β	6.62	7.11/6.38	7.11/6.43	7.08	6.37/5.67	6.40/5.71
CH^-	3.45 [b]	5.47	5.41	3.93 [b]	4.44	4.42
$^1J(^{13}C–^1H)$ (Hz)	128.5	150.5	147.9	127.8	147.5	149.6

[a] run in d_8-THF [b] CH_2.

Furthermore, separation of the pyridyl α and β resonances into two distinct sets occurs, with no merging of these resonances witnessed as high as 340 K. Taken together, these data suggest that in solution these complexes mirror their solid-state structures, that is, the negative charge has moved to the ring nitrogen, the pyridyl ring has lost aromaticity, the C_γ–CH unit has double bond character and the sp^2 nature of the CH unit holds the phenyl ring to one side, making the two sides of the pyridyl ring inequivalent. The NMR spectra of polymeric **7Na·PMDETA** and **7K·PMDETA** recorded in d_8-THF, imply their structures breakdown to THF-solvated monomers in this medium as the PMDETA resonances represent free ligands. Although the chemical shifts cannot be compared with those of the C_6D_6 solutions, the same patterns emerge such as the splitting of α and β pyridyl protons into distinct resonances, indicative of asymmetry and thus lack of rotation for the benzyl group. The $^1J(^{13}C–^1H)$ coupling constants for the formally metallated CH groups fall in the narrow range of 147.5–150.5 Hz regardless of NMR solvent, which indicates a similar hybridization lying towards the sp^2 end of the spectrum.

DFT Analysis

Further insight into the coordination modes of the alkali metals cations to the arylmethyl anions was gained from DFT calculations [B3LYP/6–311 + G(d)], in conjunction with detailed NBO, NICS(1) and QTAIM analyses of the resulting electronic structures of these complexes. The optimised geometrical parameters of all model structures are in good agreement with their crystallographic counterparts, and general structural trends are well replicated by the calculations. Stronger cation-anion interactions at the expense of weaker cation-ligand bonding observed in the DFT-optimised geometries can be attributed to dominant electrostatic contributions to the overall binding. Exemplary structures of Na^+ interacting with all arylmethyl anions are depicted in Figure 18. A comprehensive summary of all data discussed below is available in the Supporting Information.

In **4Li·PMDETA** and **4M·Me$_6$TREN** (M = Na, K) the alkali metal primarily interacts with the distorted trigonal-pyramidal C_α position of the diphenylmethyl anion in a σ-fashion. Interaction with the phenyl ring through π-coordination to the aromatic ring is energetically unfavourable: in **4Li·PMDETA** the η^6-coordinated geometry lies 16 kcal mol^{-1} higher in energy than the ground state. Unsurprisingly, across the series the M–C_α bond distance increases with the alkali ion radius (2.23–2.98 Å). The larger radius of K^+ in **4K·Me$_6$TREN** causes this ion to drift towards the centre above the "C_5 bay region" involving the *ortho*- and *ipso*-carbons of both phenyl rings as well as the C_α bridge atom. The more evenly dispersed M–C_α and M–C_{ipso} bond distances (Δ = 0.14 and 0.23 Å) in **4K·Me$_6$TREN** compared

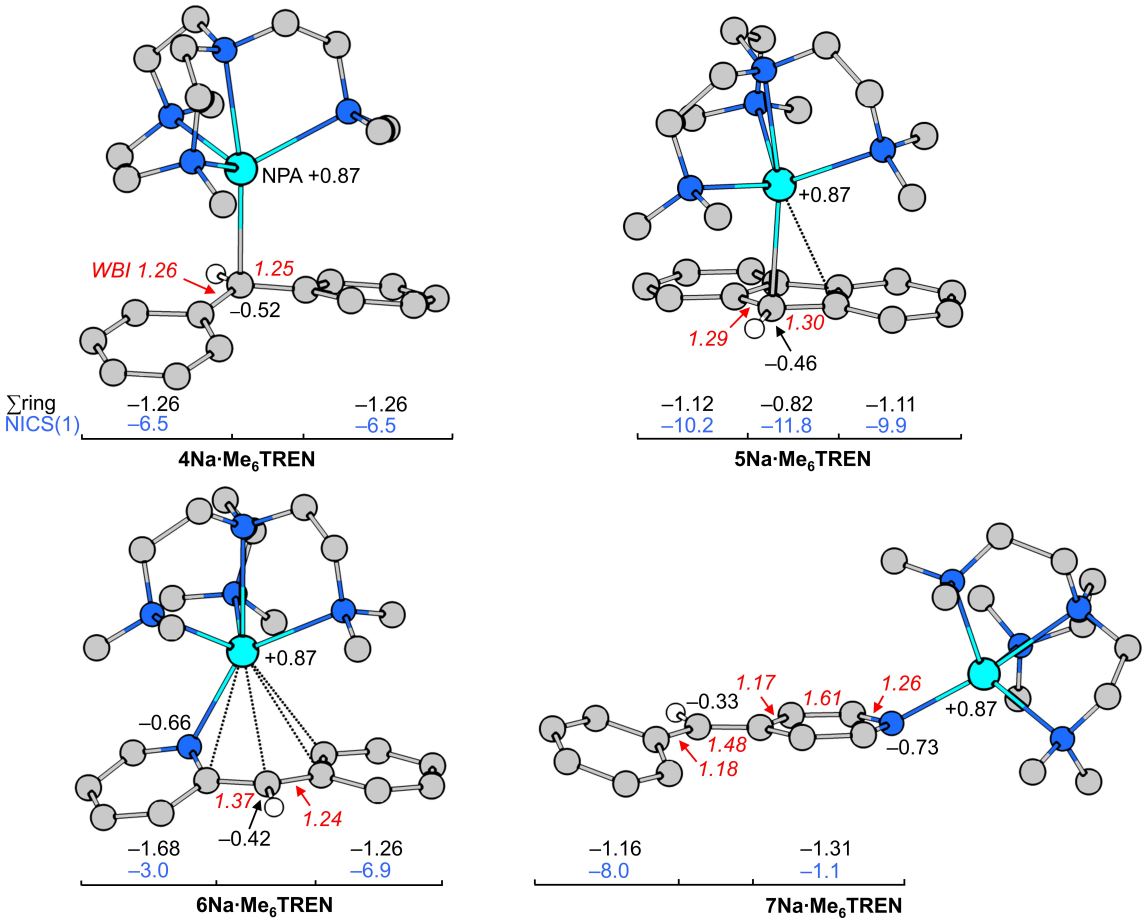

Figure 18. Optimised molecular geometries of **XNa·Me$_6$TREN** (X = **4**–**7**) along with NPA charges (black), Wiberg Bond Indices (red) and NICS(1) indices (blue, in ppm). Hydrogen atoms have been omitted for clarity (except on methine bridge).

to the Li and Na homologues (Δ = 0.49–0.68 Å) are consistent with η^3-coordination of K^+ to these atoms. Likewise, the C_α in **4K·Me$_6$TREN** adopts a more planar geometry (sum of angles 360° vs. 354° in **4Li·PMDETA**, and **4Na·Me$_6$TREN**). Across the series the C_α–C_{ipso} distances decrease marginally from 1.45 Å in **4Li·PMDETA** to 1.43 Å in **4K·Me$_6$TREN**, implying some redistribution of negative charge onto the aromatic rings. Indeed, across the series the charge decrease on CH (−0.59e in **4Li·PMDETA** to −0.44e in **4K·Me$_6$TREN**) is offset by an increase of negative charge by the same order of magnitude on the two rings, as probed by Natural Population Analysis (NPA). The slight increase of the NPA charge on the alkali metal can be attributed to the increase in electropositive character. The redistribution of charge onto the phenyl rings is paralleled by a decrease of aromaticity as reflected in the NICS(1) index (changing from −6.8/−6.7 to −5.9/−5.5 ppm). The slight asymmetry in charge accumulation with a predominance for the $C_{o'}$ positions can be rationalised with the increased contact of the potassium ion with this region. The QTAIM molecular graphs for the three structures return distinct bond paths and BCPs between each alkali-metal ion and the exocyclic C_α centre. The parameters of the M–C_α BCPs in all three complexes are consistent with closed-shell interactions [$\rho(r)$ = 0.015−0.023 a.u., $\nabla^2\rho(r)$ = 0.049–0.095 a.u. and $H(r)$ = 0.001–0.002 a.u.], reflecting the predominant ionic interaction of the metal with C_α. It is noteworthy that the K–C_α bond path is more angled, a result of shift of the K^+ ion towards the centre of the bay region. The small increase of the values of all parameters associated with the BCPs of the C_α–C_{ipso} linkages ($\varepsilon(r)$ = 0.213–0.245, $\rho(r)$ = 0.273–0.285 a.u., $\nabla^2\rho(r)$ = −0.662–(−0.714) a.u. and $H(r)$ = −0.248–(−0.270) a.u.) is also consistent with delocalisation of negative charge from C_α onto both phenyl rings, as is the increase of the WBI of both C_α–C_{ipso} linkages (1.22 to 1.30).

Turning to the fluorenyl complexes, the structural trends observed in **5Li·PMDETA** and **5M·Me$_6$TREN** (M = Na, K) resemble those of the diphenylmethyl complexes, that is, a drift of the alkali metal to a more central position above the central Cp ring as the ionic radii increases down the group. The calculated M–C_{Cp} bond distances for **5Na·Me$_6$TREN** support a η^2-bonding mode of Na^+ to C_α and one of the adjacent C_{ipso} centres, while in **5K·Me$_6$TREN** the evenly dispersed M–C_{Cp} distances are clearly indicative of an η^5–Cp coordination. For **5Na·Me$_6$TREN** a η^6-phenyl coordinated structure is 4 kcal mol^{-1} higher in energy, while the corresponding structure for the K^+ homologue reverses back to the η^5–Cp geometry. In contrast, the optimized geometry of **5Li·PMDETA** features a close

interaction between Li^+ and the C_α position (2.24 Å), although a slight asymmetry is also noted from the tilt of the Li(PMDETA) unit towards one C_{ipso} carbon. While in this structure Li^+ clearly lies outside the Cp ring, a η^5-bonded geometry analogous to monomeric **5Na·PMDETA**,[16] is energetically close (2.4 kcal mol^{-1}). The aromatic nature of the Cp unit of the fluorenyl anion is supported by its NICS(1) index, which slightly increases (−11.1 ppm to −12.5 ppm) as more symmetrical charge delocalisation along the ring perimeter is reached across the series.[34] The NPA charge on C_α decreases from −0.54e in **5Li·PMDETA** to −0.39e in **5K·Me$_6$TREN**, indicating charge redistribution as the hapticity of the Cp ring is changed. However, some charge is also dissipated onto the fused phenyl rings, which is in line with the observed NMR chemical shifts. The molecular graphs for **5Li·PMDETA**, **5Na·Me$_6$TREN** and **5K·Me$_6$TREN** also evidence the change in hapticity across the series, although the situation is not as clear-cut as expected. It has been pointed out that the number of M–C bond paths predicted by QTAIM analysis of metal-ring interactions is often inconsistent with the expected hapticity due to topological instabilities resulting from low electron densities.[35] The topological parameters for the Cp ring signal significant covalency in all cases. One bond path between the alkali-metal ion and C_α is found in each of **5Li·PMDETA** and **5Na·Me$_6$TREN**, indicating that this is the dominant interaction in both cases. Three bond paths and associated bond/ring critical points (K–C_α, K–C_o, K–$C_{o'}$) are seen for **5K·Me$_6$TREN**, unequivocally signalling the general trend of a change in hapticity across the series.

The Na–N_{py} (2.54 Å) and Na–C_α (3.10 Å) bond distances in the optimised geometry of **6Na·Me$_6$TREN** suggest that the interaction with the Na^+ centre occurs predominantly through the N_{py} donor of the pyridyl ring. The pyridyl moiety is slightly rotated out of plane (dihedral angles 25°), *cis* to the Ph ring. The alternative *trans* conformer, in which the Ph ring lies *trans* to the N atom, is energetically destabilised by 15 kcal mol^{-1}. Meanwhile, the C_α–C_{ipso} and C_α–C_2 bond distances in optimised **6Na·Me$_6$TREN** are asymmetrical: a slightly longer distance of 1.44 Å is associated with the benzyl linkage, while the bonds towards pyridyl are shortened to 1.41 Å. Taken together with the remaining ligand bond lengths, this situation is diagnostic of an enamide resonance form that localises negative charge onto the nitrogen atom. Across the series, the C_α–C_{ipso} bond slightly lengthens, and aza-allyl character becomes dominant in **6K·Me$_6$TREN**. Concomitantly, the potassium establishes close contacts with the three atoms of the aza-allyl unit (M–N_{py} 2.85 Å, M–C_α 3.10 Å and M–C_2 3.15 Å). That notwithstanding, short K–C_{ipso} (3.14 Å) and K–C_{ortho} (3.16 Å) distances indicate that bonding interactions also exist between the C_{ipso} and C_{ortho} centres and K^+. Collectively, NPA charges, Wiberg bond orders and QTAIM topological parameters consolidate the above interpretation of the structural changes. In all complexes the negative charge is mostly located on the pyridyl ring (~ −1.70e > ~ −1.26e on phenyl). The C_α–C_{ipso} bond within the benzyl moiety maintains its single bond character (WBI: 1.22–1.25, $\varepsilon(r)$: 0.189–0.211 a.u.), whilst the linkage between pyridyl and C_α transitions from a localised double bond towards a more delocalised situation (WBI: 1.42–1.35, $\varepsilon(r)$: 0.301–0.279 a.u.). NICS(1) indices are also consistent with the above observations, showing that the phenyl ring maintains its aromatic character in all complexes (falling between −6.9 and −6.5 ppm). The QTAIM molecular graphs give further insight: **6M·Me$_6$TREN** (M = Li, Na) reveal bond paths and bond critical points between the alkali metals and N_{py}, whilst two bond paths (K–N_{py}, K–C_α) are observed for M = K, tracing a ring structure between these three atoms. Taken together, these data are consistent with a transition from enamide bonding for the Li homologue to aza-allyl bonding in the potassium complex.

Coordination of the Na ion in **7Na·Me$_6$TREN** to the N donor of the phenyl(4-pyridyl)methyl ligand, is energetically preferred over coordination to the methine carbon by 2 kcal mol^{-1}. In agreement with experiment, the optimised Na–N bond distance (2.32 Å) is significantly contracted relative to **6Na·Me$_6$TREN** (2.54 Å). The pattern of optimised bond parameters in the pyridyl ring is indicative of "quinoidal-type" conjugation, with significant double bond character in the C_α–C_4, C_2–C_3 and C_5–C_6 linkages of the pyridine ring. The ellipticities and bond orders associated with the pyridine ring ($\varepsilon(r)$: 0.295–0.302 a.u.; WBI: 1.48–1.61) are also diagnostic of this bond conjugation. Significant charge localisation onto the nitrogen donor via this pathway is evident from the NPA analysis (−0.73e). The Na–N interaction is predominantly ionic in character as evident from the QTAIM parameters at its BCP [$\rho(r) = 0.026$ a.u., $\nabla^2\rho(r) = 0.146$ a.u. and $H(r) = 0.005$ a.u.]. Loss of aromaticity of the pyridine ring is again reflected in the associated NICS(1) index (−1.1 ppm), as compared to the phenyl ring which maintains its aromatic character (−8.0 ppm). A survey of possible coordination modes for all metal ions (see Table S9, Fig S47) reveals similar trends as for the other ditopic anions: for Me$_6$TREN *N*-coordination is energetically preferred for Li^+ and Na^+, whilst coordination to either pyridine or the C_5 unit become favourable for K^+. With the more flexible PMDETA ligand, different coordination modes appear to be energetically accessible, but *N*-coordination remains preferred for Li^+. The above result is in line with the experimentally determined structure of **7Na·PMDETA**. Using a fragment-based structural model of its crystallographic structure (see Supporting Information for details) negative charge accumulates on both C_α (−0.40e) and N_{py} (−0.72e) due to polarisation by Na^+ ions. This charge distribution enables formation of a polymer. Bond critical paths between Na^+ and both donor atoms in the molecular graph along with QTAIM parameters [$\rho(r) = 0.010$–0.022 a.u., $\nabla^2\rho(r) = 0.042$–0.121 a.u. and $H(r) = 0.002$–0.004 a.u.] at their respective BCPs signal ionic interactions between these centres. The shift in charge as compared to that in the monomeric counterpart in this structure is also reflected in a slight increase in the aromaticity of the pyridine and phenyl rings. Their NICS(1) values of −8.2 and −2.0 ppm can be compared to those in monomeric *N*-coordinated **7Na·PMDETA** (−8.0 and −0.9 ppm).

Conclusions

In summary, we have successfully synthesised target monomeric lithium, sodium and potassium diphenylmethyl, fluorenyl, phenyl(2-pyridyl)methyl and phenyl(4-pyridyl)methyl complexes and characterized these by solution NMR spectroscopy, DFT calculations and where possible by XRD. The presence of the second aromatic ring in the diphenylmethyl ligand provides more area over which to delocalise the negative charge arising from metallation of the CH_2 bridge of diphenylmethane and so the σ to π migration of the metal is far less pronounced than that in the monosubstituted phenylmethyl (benzyl) derivatives. Tethering the two aromatic rings together as found in fluorenyl promotes π-type coordination since the anion contains a third central aromatic (cyclopentadienyl) ring for binding metals, which on coordination produce half-sandwich type geometries, although the hapticity of the interaction does increase with increasing ionic radius of the metal. DFT calculations support the interpretation that phenyl(2-pyridyl)methyl moves from an enamide formation at one extremity (lithium) to an aza-allyl formation at the other extremity (potassium) through the presence of a bond between the formally carbanionic carbon and K, although in all cases the phenyl ring lies *cis* to the ring nitrogen with respect to the C_2–C_α bond rather than *trans*. The phenyl(4-pyridyl)methyl ligand preferentially reorganises to an enamide formation in the monomer (Li, Na) but utilizing a smaller tridentate donor in the form of PMDETA leads to polymeric structures for heavier alkali-metals with both M–C_α and M–N interactions which propagates the chain.

Deposition Numbers

2124368 (for **4Li·PMDETA**), 2124369 (for **4Na·Me$_6$TREN**), 2124370 (for **4K·Me$_6$TREN**), 2124371 (for **5Na·Me$_6$TREN**), 2124372 (for **5K·Me$_6$TREN**), 2124373 (for **6Na·Me$_6$TREN**), 2124374 (for **7Na·Me$_6$TREN**), 2124375 (for **7Na·PMDETA**) contain the supplementary crystallographic data for this paper. These data are provided free of charge by the joint Cambridge Crystallographic Data Centre and Fachinformationszentrum Karlsruhe Access Structures service.

Acknowledgements

AR thanks the University of Strathclyde for a PhD studentship through the Strathclyde Centre for Doctoral Training. KMB and TK acknowledge the Irish Centre for High-End Computing (ICHEC) for the provision of computational facilities and support.

Conflict of Interest

The authors declare no conflict of interest.

Data Availability Statement

The data that support the findings of this study are available in the supplementary material of this article.

Keywords: alkali-metals · arene ligands · density functional calculations · pi interactions · x-ray diffraction

[1] U. Wietelmann, J. Klett, *Z. Anorg. Allg. Chem.* **2018**, *644*, 194–204.
[2] a) B. J. Wakefield, *The chemistry of organolithium compounds*, Pergamon, Oxford, **1974**; b) J. Clayden, *Organolithiums: selectivity for synthesis*, Pergamon, Oxford, **2002**; c) Z. Rappoport, I. Marek, *The chemistry of organolithium compounds*, Wiley, Chichester, **2005**; d) V. H. Gessner, C. Däschlein, C. Strohmann, *Chem. Eur. J.* **2009**, *15*, 3320–3334; e) *Organometallics in Synthesis: Third Manual*, Wiley, Hoboken, **2013**; f) *Lithium Compounds in Organic Synthesis - From Fundamentals to Applications*, Wiley-VCH, **2014**; g) D. C. Kail, P. M. Krizkova, A. Wieczorek, F. Hammerschmidt, *Chem. Eur. J.* **2014**, *20*, 4086–4091; h) V. Capriati, F. M. Perna, A. Salomone, *Dalton Trans.* **2014**, *43*, 14204–14210.
[3] a) W. Clegg, B. Conway, A. R. Kennedy, J. Klett, R. E. Mulvey, L. Russo, *Eur. J. Inorg. Chem.* **2011**, 721–726; b) C. Glock, H. Görls, M. Westerhausen, *Eur. J. Inorg. Chem.* **2011**, 5288–5298; c) A. Ojeda-Amador, A. J. Martinez-Martinez, G. M. Robertson, S. D. Robertson, A. R. Kennedy, C. T. O'Hara, *Dalton Trans.* **2017**, *46*, 6392–6403; d) S. Asako, H. Nakajima, K. Takai, *Nature Catalysis* **2019**, *2*, 297–303; e) S. Asako, M. Kodera, H. Nakajima, K. Takai, *Adv. Synth. Catal.* **2019**, *361*, 3120–3123; f) R. A. Woltornist, Y. Ma, R. F. Algera, Y. Zhou, Z. Zhang, D. B. Collum, *Synthesis* **2020**, *52*, 1478–1488; g) J. H. Harenberg, N. Weidmann, P. Knochel, *Angew. Chem. Int. Ed.* **2020**, *59*, 12321–12325; *Angew. Chem.* **2020**, *132*, 12419–12424; h) J. H. Harenberg, N. Weidmann, K. Karaghiosoff, P. Knochel, *Angew. Chem. Int. Ed.* **2021**, *60*, 731–735; *Angew. Chem.* **2021**, *133*, 742–746; i) S. Asako, I. Takahashi, H. Nakajima, L. Ilies, K. Takai, *Commun. Chem.* **2021**, *4*, 76.
[4] a) D. L. Anderson, *J. Geophys. Res.* **1983**, *88*, B41–B52; b) P. C. K. Vesborg, T. F. Jaramillo, *RSC Adv.* **2012**, *2*, 7933–7947.
[5] a) D. Larcher, J.-M. Tarascon, *Nat. Chem.* **2015**, *7*, 19–29; b) N. Nitta, F. Wu, J. T. Lee, G. Yushin, *Mater. Today* **2015**, *18*, 252–264; c) T. Kim, W. Song, D.-Y. Son, L. K. Ono, Y. Qi, *J. Mater. Chem. A* **2019**, *7*, 2942–2964.
[6] S. Wappelhorst, H. Cui.
[7] a) Y. Suzuki, S. Ishida, S. Sato, H. Isobe, T. Iwamoto, *Angew. Chem. Int. Ed.* **2017**, *56*, 4593–4597; *Angew. Chem.* **2017**, *129*, 4664–4668; b) J. Hicks, P. Vasko, J. M. Goicoechea, S. Aldridge, *Nature* **2018**, *557*, 92–95; c) R. J. Schwamm, M. D. Anker, M. Lein, M. P. Coles, *Angew. Chem. Int. Ed.* **2019**, *58*, 1489–1493; *Angew. Chem.* **2019**, *131*, 1503–1507; d) R. J. Schwamm, M. P. Coles, M. S. Hill, M. F. Mahon, C. L. McMullin, N. A. Rajabi, A. S. S. Wilson, *Angew. Chem. Int. Ed.* **2020**, *59*, 3928–3932; *Angew. Chem.* **2020**, *132*, 3956–3960; e) S. Grams, J. Eyselein, J. Langer, C. Färber, S. Harder, *Angew. Chem. Int. Ed.* **2020**, *59*, 15982–15986; *Angew. Chem.* **2020**, *132*, 16116–16120; f) S. Kurumada, S. Takamori, M. Yamashita, *Nat. Chem.* **2020**, *12*, 36–39.
[8] a) J. M. Smith, A. R. Sadique, T. R. Cundari, K. R. Rodgers, G. Lukat-Rodgers, R. J. Lachicotte, C. J. Flaschenriem, J. Vela, P. L. Holland, *J. Am. Chem. Soc.* **2006**, *128*, 756–769; b) M. M. Rodriguez, E. Bill, W. W. Brennessel, P. L. Holland, *Science* **2011**, *334*, 780–783; c) M. D. Anker, M. P. Coles, *Angew. Chem. Int. Ed.* **2019**, *58*, 18261–18265; *Angew. Chem.* **2019**, *131*, 18429–18433; d) J. Hicks, A. Heilmann, P. Vasko, J. M. Goicoechea, S. Aldridge, *Angew. Chem. Int. Ed.* **2019**, *58*, 17265–17268; *Angew. Chem.* **2019**, *131*, 17425–17428; e) M.-A. Legare, G. Belanger-Chabot, R. D. Dewhurst, E. Welz, I. Krummenacher, B. Engels, H. Braunschweig, *Science* **2018**, *359*, 896–900.
[9] a) M. G. Davidson, D. Garcia-Vivo, A. R. Kennedy, R. E. Mulvey, S. D. Robertson, *Chem. Eur. J.* **2011**, *17*, 3364–3369; b) D. R. Armstrong, M. G. Davidson, D. Garcia-Vivo, A. R. Kennedy, R. E. Mulvey, S. D. Robertson, *Inorg. Chem.* **2013**, *52*, 12023–12032; c) A. R. Kennedy, R. E. Mulvey, R. I. Urquhart, S. D. Robertson, *Dalton Trans.* **2014**, *43*, 14265–14274.
[10] a) M. M. Olmstead, P. P. Power, *J. Am. Chem. Soc.* **1985**, *107*, 2174–2175; b) S. Neander, F. E. Tio, R. Buschmann, U. Behrens, F. Olbrich, *J. Organomet. Chem.* **1999**, *582*, 58–65; c) S. Neander, J. Körnich, F. Olbrich, *J. Organomet. Chem.* **2002**, *656*, 89–96; d) I. Fernandez, E. Martinez-Viviente, F. Breher, P. S. Pregosin, *Chem. Eur. J.* **2005**, *11*, 1495–1506; e) J. S. Alexander, D. G. Allis, W. Teng, K. Ruhlandt-Senge, *Chem. Eur. J.* **2007**, *13*, 9899–9911.

[11] A. Zaeni, U. Behrens, P. Liebing, F. Olbrich, F. T. Edelmann, *J. Organomet. Chem.* **2017**, *830*, 141–145.
[12] C. Üffing, R. Köppe, H. Schnöckel, *Organometallics* **1998**, *17*, 3512–3515.
[13] R. E. Dinnebier, S. Neander, U. Behrens, F. Olbrich, *Organometallics* **1999**, *18*, 2915–2918.
[14] M. Håkansson, C.-H. Ottosson, A. Boman, D. Johnels, *Organometallics* **1998**, *17*, 1208–1214.
[15] J. J. Brooks, W. Rhine, G. D. Stucky, *J. Am. Chem. Soc.* **1972**, *94*, 7339–7346.
[16] S. Corbelin, J. Kopf, E. Weiss, *Chem. Ber.* **1991**, *124*, 2417–2422.
[17] C. Janiak, *Chem. Ber.* **1993**, *126*, 1603–1607.
[18] S. Corbelin, N. P. Lorenzen, J. Kopf, E. Weiss, *J. Organomet. Chem.* **1991**, *415*, 293–313.
[19] M. Könemann, G. Erker, R. Fröhlich, E.-U. Würthwein, *J. Am. Chem. Soc.* **1997**, *119*, 11155–11164.
[20] H. Schumann, D. M. M. Freckmann, S. Dechert, *Organometallics* **2006**, *25*, 2696–2699.
[21] R. Zerger, W. Rhine, G. D. Stucky, *J. Am. Chem. Soc.* **1974**, *96*, 5441–5448.
[22] U. Behrens, S. May, F. Olbrich, *Z. Kristallogr.* **2007**, *222*, 307–309.
[23] S. Buchholz, K. Harms, M. Marsch, W. Massa, G. Boche, *Angew. Chem. Int. Ed. Engl.* **1989**, *28*, 72–73.
[24] W.-P. Leung, L.-H. Weng, R.-J. Wang, T. C. W. Mak, *Organometallics* **1995**, *14*, 4832–4836.
[25] H.-H. Giese, T. Habereder, H. Nöth, W. Ponikwar, S. Thomas, M. Warchhold, *Inorg. Chem.* **1999**, *38*, 4188–4196.
[26] a) L. Lochmann, J. Pospišil, D. Lim, *Tetrahedron Lett.* **1966**, *7*, 257–262; b) M. Schlosser, *J. Organomet. Chem.* **1967**, *8*, 9–16.
[27] T. Tatic, S. Hermann, M. John, A. Loquet, A. Lange, D. Stalke, *Angew. Chem. Int. Ed.* **2011**, *50*, 6666–6669; *Angew. Chem.* **2011**, *123*, 6796–6799.
[28] W. Zarges, M. Marsch, K. Harms, G. Boche, *Chem. Ber.* **1989**, *122*, 2303–2309.
[29] S. Bachmann, B. Gernert, D. Stalke, *Chem. Commun.* **2016**, *52*, 12861–12864.
[30] a) H. Ott, U. Pieper, D. Leusser, U. Flierler, J. Henn, D. Stalke, *Angew. Chem. Int. Ed.* **2009**, *48*, 2978–2982; *Angew. Chem.* **2009**, *121*, 3022–3026; b) E. V. Brouillet, A. R. Kennedy, T. Krämer, R. E. Mulvey, S. D. Robertson, A. Stewart, S. Towie, *Z. Anorg. Allg. Chem.* **2020**, *646*, 726–733.
[31] U. Pieper, D. Stalke, *Organometallics* **1993**, *12*, 1201–1206.
[32] a) D. M. Cousins, M. G. Davidson, C. J. Frankis, D. Garcia-Vivo, M. F. Mahon, *Dalton Trans.* **2010**, *39*, 8278–8280; b) S. D. Robertson, A. R. Kennedy, J. J. Liggat, R. E. Mulvey, *Chem. Commun.* **2015**, *51*, 5452–5455; c) D. R. Armstrong, C. M. M. Harris, A. R. Kennedy, J. J. Liggat, R. McLellan, R. E. Mulvey, M. D. T. Urquhart, S. D. Robertson, *Chem. Eur. J.* **2015**, *21*, 14410–14420.
[33] R. E. Mulvey, S. D. Robertson, *Angew. Chem. Int. Ed.* **2013**, *52*, 11470–11487; *Angew. Chem.* **2013**, *125*, 11682–11700.
[34] C. Foroutan-Nejad, S. Shahbazian, P. Rashidi-Ranjbar, *Phys. Chem. Chem. Phys.* **2010**, *12*, 12630–12637.
[35] L. J. Farrugia, C. Evans, D. Lentz, M. Roemer, *J. Am. Chem. Soc.* **2009**, *131*, 1251–1268.

Manuscript received: November 29, 2021
Accepted manuscript online: February 16, 2022
Version of record online: March 8, 2022